Final Report: Biomechanical evaluation of the Titania cervical intervertebral disc prosthesis

Investigators:
Neil R. Crawford, PhD
Kemal Yücesoy, MD
K. Zafer Yüksel, MD
Felix Dominguez, MD
Phillip M. Reyes, BSE
Anna G.U. Sawa, MS

Spinal Biomechanics Research Laboratory
Barrow Neurological Institute
St. Joseph's Hospital & Medical Center
Phoenix, Arizona

Prepared for:
Meteor Medical
November 24, 2010

Contents

Introduction

Several experiments have been performed in recent years to study the biomechanics of artificial discs implanted in the cervical spine (Crawford, 2006). Most of these experiments have had a narrow focus, studying primarily the effect of devices on the spine's range of motion (Table 1). We proposed and performed a multifaceted experiment to quantify a number of previously poorly documented experimental parameters characterizing the biomechanics of the cervical spine before and after insertion of Meteor Medical's Titania cervical disc prosthesis (Figure 1). Few published studies to date have reported an array of parameters as large as in this protocol, especially the axis of rotation, a key parameter. It was hypothesized that after insertion of the Titania artificial disc, there would be only minimal alteration to these biomechanical parameters compared to the intact spine. As a negative control, spines were also studied in the plated condition.

Table 1. Laboratory studies of artificial discs in which some biomechanical parameters included in this protocol have been reported.

Parameter	Lab Studies Reported
Range of Motion	(1) McAfee et al. 2003 (2) Puttlitz et al. 2004 (3) Dmitriev et al. 2005 (4) Kotani et al. 2005 (5) Hu et al. 2006 (6) Chang et al. 2007b
Angular Coupling	(1) Puttlitz et al. 2004
Segmental Angle Contribution	(1) DiAngelo et al. 2003 (2) DiAngelo et al. 2004
Neutral or Lax Zone	(1) Kotani et al. 2005 (2) Dmitriev et al. 2005
Axis of Rotation	(none)
Facet Load	(1) Chang et al. 2007a*

**Although "facet load" was reported by Chang et al., results are questionable since only one strain gauge was applied*

Methods

Eight human cadaveric C3-T1 specimens were studied (Table 2). Specimens were obtained fresh frozen then thawed in a bath of normal saline at 30°C and carefully cleaned of muscle tissue without damaging any ligaments, discs, or joint capsules. Plain film x-rays were taken and specimens with any obvious flaws (especially metastatic disease, osteophytes, disc narrowing, or joint arthrosis) were excluded and replaced. Anteroposterior dual energy x-ray absorptiometry (DEXA) scans were performed on the C4 vertebra of each specimen to assess bone mineral density (BMD). Specimens with scores indicating obvious osteoporosis were excluded and replaced. For testing, screws were inserted in the exposed endplates and facet articulations, and the heads of the screws were potted in polymethylmethacrylate (PMMA) in metal fixtures. Arrays of four uniaxial strain gauges were mounted on the left and right laminae of C5 near the C5-C6 facet joints (Figure 2). Gauges were glued to the bone with their axes aligned with the predicted primary strain direction. After applying gauges, a rigid guide wire was inserted in the lamina or spinous process and the electrical leads for the gauges were glued to this wire to serve as “strain relief,” ensuring that leads would not deform and affect strain gauge readings during testing (Figure 2).

Table 2. Specimen information.

Specimen No.	Specimen ID	Gender	Age (years)	BMD (g/cm^2)	Device Size (mm)	Plate Size (mm)
TI01	766	M	50	0.555	?	?
TI02	760	M	43	0.478	6.5	25
TI03	813	F	45	0.793	5.5	?
TI04	810	F	39	0.614	6.5	25
TI05	809	F	54	0.566	7	27.5
TI06	811	M	47	0.584	6.5	27.5
TI07	815	F	48	0.579	7	27.5
TI08	689	M	62	0.430	6.5	27.5
		Mean±SD	49±7	0.575±0.107		

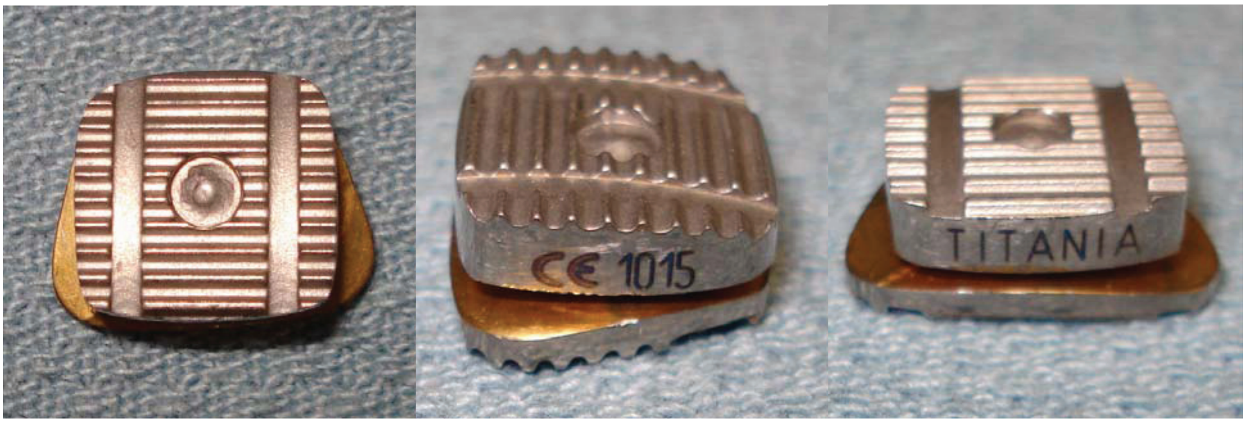

Figure 1. The Titania cervical disc prosthesis is an articulating joint with central post. Teeth on the endplates hold the device in place for stable plate-bone interface.

Figure 2. Photograph (posterior view) of specimen showing how two 4-gauge pads of uniaxial strain gauges (arrows) were applied on the left and right laminae near the inferior articular processes of C5 for measurement of C5-C6 facet loads. Each pad was oriented diagonally so that the gauge axes were along the predicted primary direction of strain. Rigid stainless steel guide wires (also visible) were inserted into the spinous process and the electrical leads for the strain gauges were glued and/or taped to the guide wires to serve as strain relief.

Specimens were tested nondestructively in the intact condition, again after inserting the disc prosthesis at C5-C6 (Figure 3a), and once more after removing the disc prosthesis, inserting a wedge graft, and applying an anterior locking plate across C5-C6 (Figure 3b), reinforced with polymethylmethacrylate.

The disc prosthesis was available in 5.5, 6.0, 6.5, and 7.0 mm heights; the appropriate size was chosen based on the anatomy of each specimen (Table 2). Prosthesis insertion was done using the manufacturer's recommended tools and procedures with the specimen positioned upright (Figure 4). Briefly, a discectomy was performed and loose disc material was scraped using a curette. Using a guide tool, reference pins were inserted into the vertebral bodies above and below the disc, leaving holes in the vertebral bodies (Figure 3a). The device was then attached as a single unit to an insertion tool and driven into place with a hammer.

After removing the disc prosthesis, no further preparation of the disc space was done before inserting a wedge graft (PEEK) and applying a locking plate (Atlantis, Medtronic, Inc.). Plate size was chosen to suit the anatomy of each specimen (Table 2). In all specimens, 4.0x14 mm screws were used to attach plates.

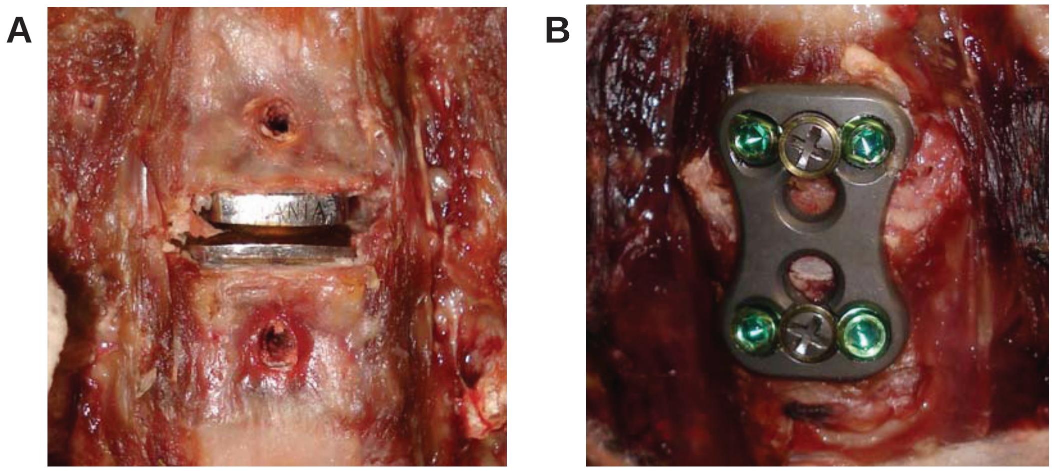

Figure 3. Instrumented conditions tested: (A) After Titania implantation (the large holes in the vertebral bodies above and below the disc are from the reference pins used for the guiding tool during disc implantation); (B) After placement of a wedge graft and a locking anterior plate.

Figure 4. To maintain the same marker calibration, device insertion was done with the specimen upright, clamped to a vise, and an assistant applying compression manually while preparing the endplates or driving the device.

In both intact and instrumented conditions, specimens were studied sequentially in two different loading apparatuses. First, for pure moment testing, an apparatus was used in which a system of cables and pulleys imparts nondestructive, nonconstraining torques in conjunction with a standard servohydraulic test system (MTS, Minneapolis, Minnesota), as described previously (Figure 5, Crawford et al., 1995). This technique gives reproducible results because a pure moment is distributed uniformly across the specimen regardless of the point of load application (Panjabi, 1988). Loads of 1.5 Nm maximum were applied about the appropriate anatomical axes to induce motion in the three primary anatomical planes: flexion, extension, left and right lateral bending, and left and right axial rotation. While applying each load, voltage recordings from each of the four strain gauges was recorded continuously.

Figure 5. Pure moment apparatus. Strings and pulleys in conjunction with a standard servohydraulic test frame were used to induce flexion, extension (shown), axial rotation, and lateral bending.

Next, for physiological flexion-extension loading, the specimens were transferred to a compression-flexion apparatus (Figure 6) in which a constant compressive follower load of 70 N is applied from a belt looped in the midsagittal plane around the specimen. In this apparatus, movement was induced until specimens reached the same C3-T1 angle (sum of C3-C4, C4-C5, C5-C6, C6-C7, and C7-T1 angles) that was previously achieved during pure moment flexibility tests for that condition. The rationale behind targeting the same angle with this more complex load that was reached with the simple (pure moment) load is that the same “muscular exertion” is theoretically created in both apparatuses; the alternative, matching a pure moment to an equivalent complex combined load, is infeasible. As with pure moment flexibility tests, the voltage

Three-dimensional specimen motion in response to the applied loads during flexibility and stiffness tests was determined using the Optotrak 3020 (Northern Digital, Waterloo, Ontario, Canada). This system measures stereophotogrammetrically the three-dimensional displacement of infrared-emitting markers rigidly attached in a noncollinear arrangement to each vertebra (Figure 7). Custom software converted the marker coordinates to angles about each of the anatomical axes in terms of the motion segment's coordinate system (Crawford and Dickman, 1997). Spinal angles were calculated using a technique that provides the most appropriate results for describing the spine's angular coupling patterns (Crawford et al., 1999).

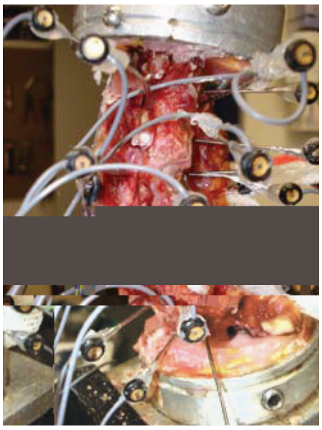

Figure 7. Optical markers for tracking specimen motion were attached to the ends of stainless steel guide wires that had been drilled into the vertebral body, lamina, or lateral mass in 3 locations per vertebra.

Testing for one specimen required 1 or 2 full days. If a second day of testing was needed, specimens were refrigerated overnight to mitigate degradation. Refreezing of specimens was avoided for fear of damaging the strain gauges. After completing all testing, the facets were disarticulated and the strain gauges were calibrated by applying a series of test loads of known magnitude using a plunger oriented normal to the C5 facet surface (Figure 8). Using these test loads in a neural net model enabled identification of the location and magnitude of forces transferred by the facets during the experiment (Sawa et al., 2008).

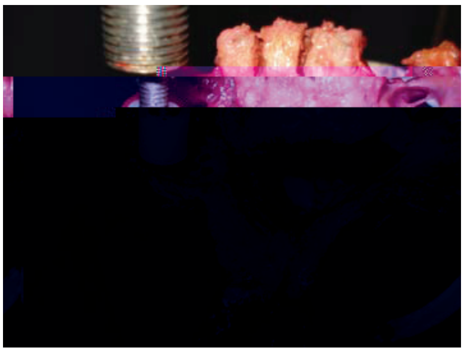

Figure 8. Calibration of strain gauges required the specimen to be disarticulated after completing testing. Then, test loads were applied using the MTS piston fitted with a plunger. Loads were applied to a series of points (shown marked with permanent ink) while recording output from each strain gauge. A neural network model used these test loads to establish the relationship between strain gauges and facet load.

From the raw data, several parameters were calculated. The angular range of motion (ROM) during motion in all planes, angular lax zone (LZ, portion of ROM in which ligaments/hardware are lax) and stiff zone (SZ, portion of the ROM in which ligaments/hardware are under tension) were determined from flexibility tests (Figure 9, Crawford et al., 1998). Also, from flexibility tests, angular coupling ratios (coupled angle under full load divided by primary angle under full load) were determined. From flexion-compression (stiffness) tests, the segmental angular contribution to global motion was determined at the global flexion or extension angles corresponding to global flexion or extension during flexibility tests. The location of the instantaneous axis of rotation during flexion and extension was determined in the midsagittal plane. Facet loads from strain gauges during loading in each direction were also determined from calibrated strain data. All data were statistically analyzed using One-Way Repeated Measures Analysis of Variance (RM-ANOVA) followed by Holm-Sidak tests to determine whether outcome measures were significantly different among the intact condition, after inserting the disc prosthesis, and after plating. P-values less than 0.05 were considered significant.

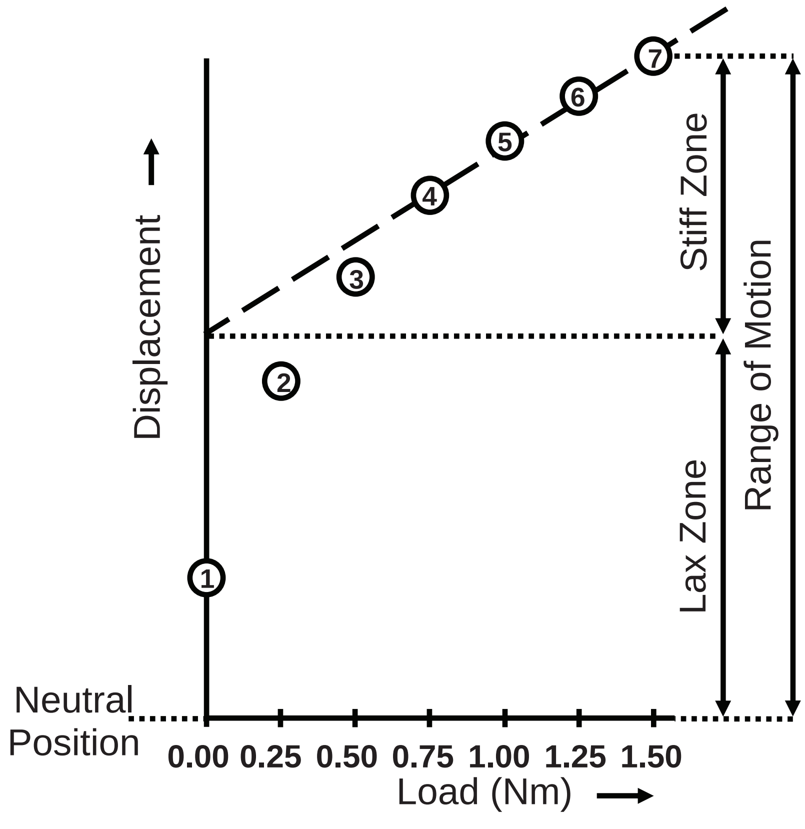

Figure 9. Schematic showing the different parameters studied. Each circle represents angular position data recorded quasistatically (after holding steady load for 45 seconds) at the seven different loads applied. The boundary between lax zone (LZ) and stiff zone (SZ) is the displacement where a line through the upper SZ is extrapolated to zero load. LZ and SZ sum to form the range of motion (ROM). Shown here is the positive half of a bidirectional motion (for example, flexion). Each positive curve has a corresponding negative curve (for example, extension). The neutral position is by definition halfway between the positive LZ/SZ boundary and the negative LZ/SZ boundary.

The location of the instantaneous axis of rotation (IAR) was calculated in 2.0º increments during motion from extension to flexion using the flexion-compression apparatus, which applies a compressive force of approximately 70N during bending. The IAR was assumed to be equivalent to the finite helical axis of motion (ignoring translation along the axis) determined from marker data using methods described by Spoor and Velpaus (1980). Before calculation of IARs, the xyz position data files were smoothed using a moving average of ±10 frames of data (smoothed frame represents average over 21 frames). This smoothing algorithm greatly reduced noise but had little effect on IAR position since movement was relatively slow (~1° per second) and data capture rate was relatively fast (~60 frames per second). After smoothing, an iterative algorithm was used to determine the next frame satisfying the requirement of >1.0° difference from the previously selected frame.

Possible relationships between shifts in IAR and other parameters were evaluated using Pearson Product Moment Correlation analysis, with a level of significance set at $p=0.05$.

Results

Surgical Technique

The first Titania disc was implanted by Dr. Kemal Yücesoy, who instructed Dr. Dominguez on the appropriate technique. All subsequent Titania discs were implanted by Dr. Dominguez. Plating after completing testing with the artificial discs in place proved to be somewhat challenging due to the presence of holes in the vertebral bodies that had been created during implantation of the artificial discs (Figure 3a). Polymethylmethacrylate was therefore used to supplement the strength of fixation by applying around the disc area and screw holes for the plate.

Range of Motion

Mean angular range of motion (ROM) at C5-C6 with the Titania disc in place was reduced to 40-62% of intact ROM during flexion, extension, lateral bending and axial rotation (Figure 10, Tables 3 and 4). This reduction was statistically significant ($p<0.001$, Table 5). The plated condition also allowed significantly less ROM than intact during all directions of loading ($p<0.001$, Table 5). The ROM was significantly less for the plated condition than with Titania in place during flexion ($p<0.002$), extension ($p=0.024$), and axial rotation ($p=0.014$), but there were no statistical difference during lateral bending ($p=0.499$, Table 5).

Table 3. Mean angular range of motion in degrees (±standard deviation).

Loading Mode	Intact	Titania	Plated
Flexion	7.33±0.89	4.51±1.53	2.23±1.80
Extension	7.33±1.23	3.70±2.44	2.03±1.66
Axial Rotation	5.76±0.83	3.45±1.11	2.50±1.36
Lateral Bending	4.95±0.70	2.00±0.70	1.81±0.91

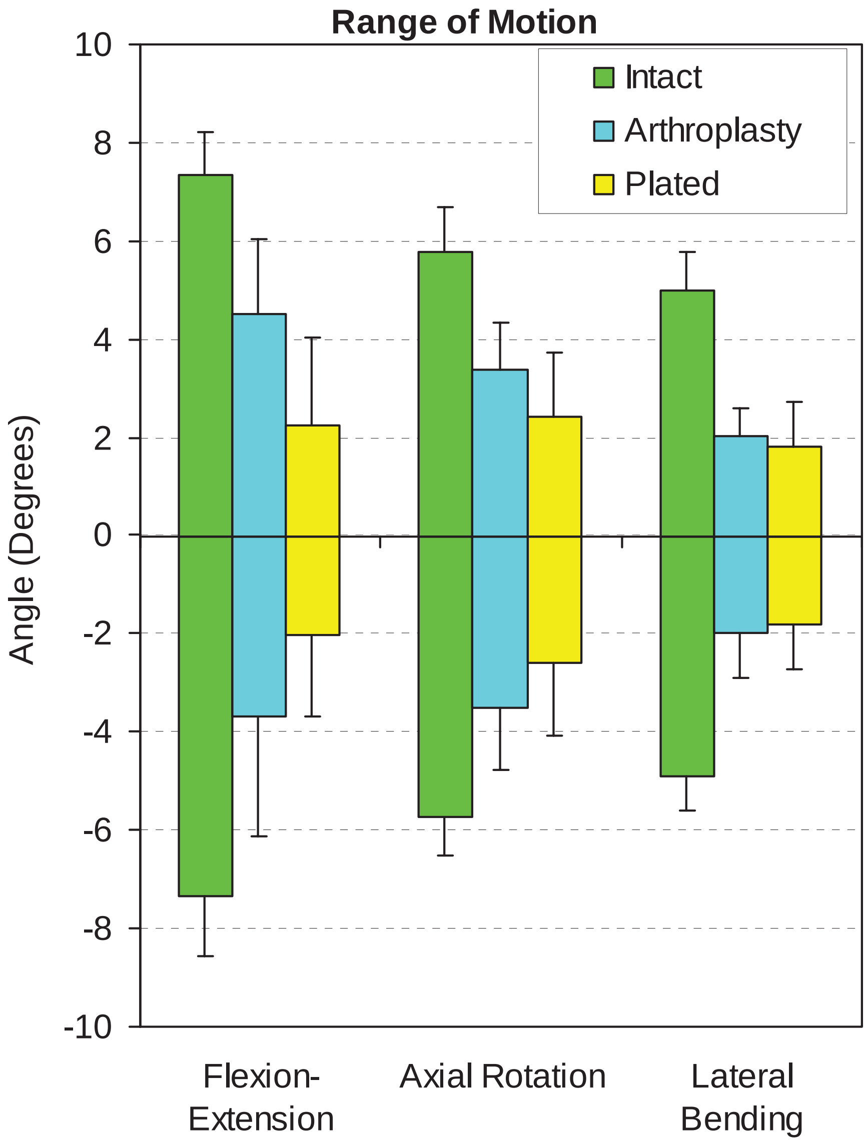

Figure 10. Mean unidirectional angular range of motion (ROM) at C5-C6 in each condition studied. Error bars show standard deviation.

Table 4. Percent difference in ROM relative to intact (±standard deviation). These differences are % of averages.

Loading Mode	Titania	Plated
Flexion	62%±22%	30%±22%
Extension	50%±32%	27%±17%
Axial Rotation	59%±18%	42%±18%
Lateral Bending	40%±11%	36%±17%

Table 5. P-values from RM-ANOVA/Holm-Sidak tests comparing mean ROM among conditions.

Flexion

	Titania	Plated
Intact	**<0.001**	**<0.001**
Titania		**0.002**

Extension

	Titania	Plated
Intact	**<0.001**	**<0.001**
Titania		**0.024**

Lateral Bending

	Titania	Plated
Intact	**<0.001**	**<0.001**
Titania		0.499

Axial Rotation

	Titania	Plated
Intact	**<0.001**	**<0.001**
Titania		**0.014**

Highlighted values represent significant differences (p<0.05).

Lax Zone

Mean angular lax zone (LZ) at C5-C6 with the Titania in place was 14-37% of intact LZ (Figure 11, Tables 6 and 7). These reductions were statistically significant ($p=<0.001$, Table 8). The plated condition also allowed significantly less LZ than intact during all directions of loading (Table 8). Titania and plated conditions did not have significantly different LZ during any loading mode ($p>0.08$, Table 8).

Table 6. Mean angular lax zone in degrees (±standard deviation).

Loading Mode	Intact	Titania	Plated
Flexion-Extension	10.03±2.28	3.57±2.44	1.88±2.52
Axial Rotation	8.60±1.55	2.55±1.43	1.87±1.56
Lateral Bending	7.52±1.39	1.12±1.04	1.15±0.94

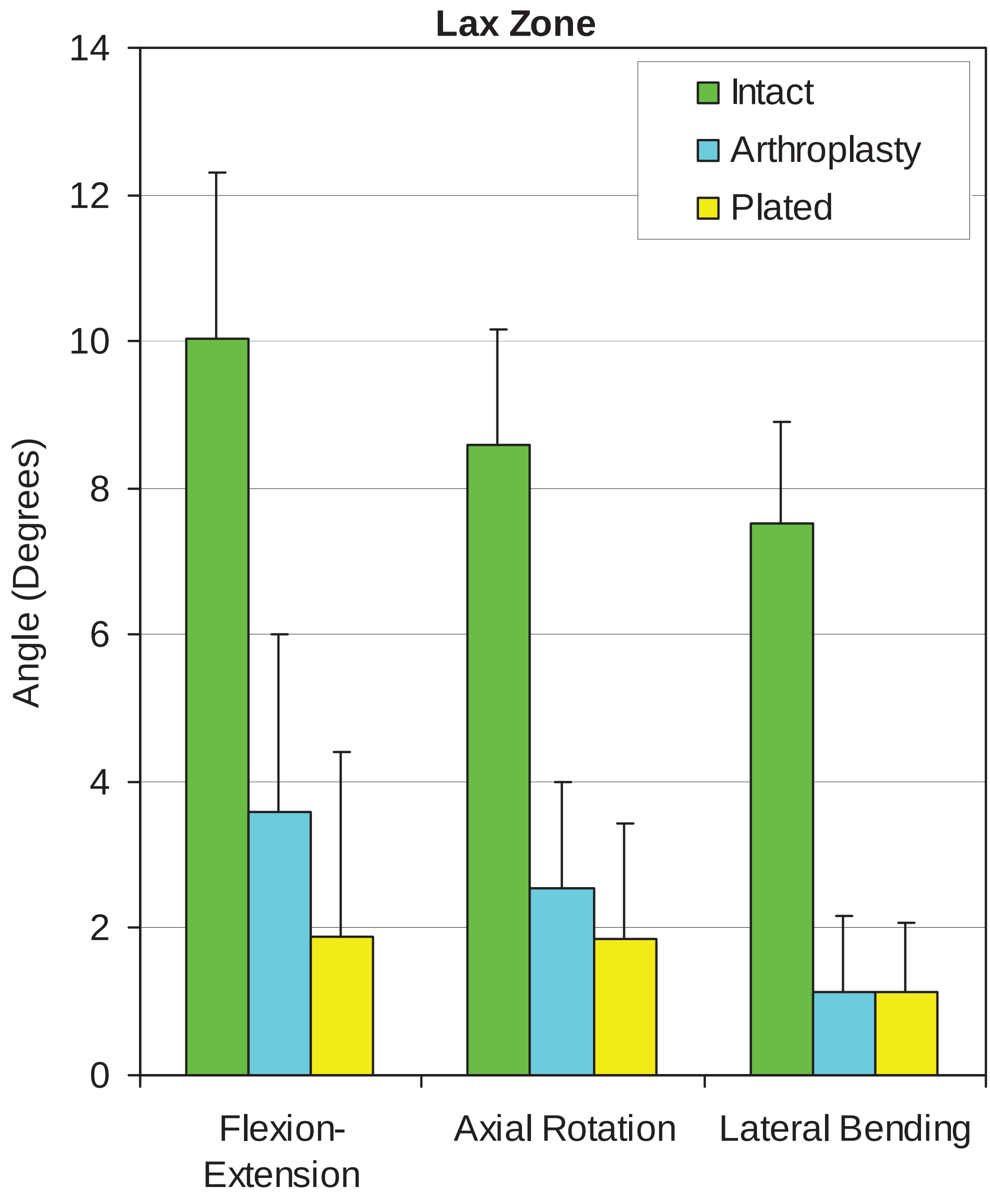

Figure 11. Mean bidirectional angular lax zone (LZ) at C5-C6 in each condition studied. Error bars show standard deviation.

Table 7. Percent difference in LZ relative to intact (±standard deviation). These differences are % of average.

Loading Mode	Titania	Plated
Flexion-Extension	37%±24%	18%±19%
Axial Rotation	30%±17%	20%±14%
Lateral Bending	14%±12%	15%±11%

Table 8. P-values from RM-ANOVA/Holm-Sidak tests comparing mean LZ among conditions.

Flexion-Extension

	Titania	Plated
Intact	**<0.001**	**<0.001**
Titania		0.087

Lateral Bending

	Titania	Plated
Intact	**<0.001**	**<0.001**
Titania		0.955

Axial Rotation

	Titania	Plated
Intact	**<0.001**	**<0.001**
Titania		0.203

Highlighted values represent significant differences ($p<0.05$).

Stiff Zone

Mean angular stiff zone (SZ) at C5-C6 with the Titania in place was less than the intact SZ during extension and greater than the intact SZ during flexion, lateral bending, and axial rotation (Figure 12, Tables 9 and 10). Of these differences, only the difference during axial rotation was statistically significant ($p<0.001$, Table 11). The plated condition allowed a SZ that was not significantly different from intact during lateral bending or axial rotation ($p>0.2$, Table 11), but significantly less than intact during flexion ($p<0.001$, Table 11) and extension ($p=0.005$, Table 11). The SZ for the plated condition was significantly less than with the Titania in place during flexion, extension and axial rotation ($p<0.05$, Table 11), while there was no statistically significant difference during lateral bending ($p=0.202$, Table 11).

Table 9. Mean angular stiff zone in degrees (±standard deviation).

Loading Mode	Intact	Titania	Plated
Flexion	2.32±0.32	2.72±0.81	1.29±0.77
Extension	2.32±0.59	1.91±1.32	1.09±0.52
Axial Rotation	1.46±0.23	2.17±0.47	1.57±0.60
Lateral Bending	1.20±0.20	1.44±0.22	1.23±0.47

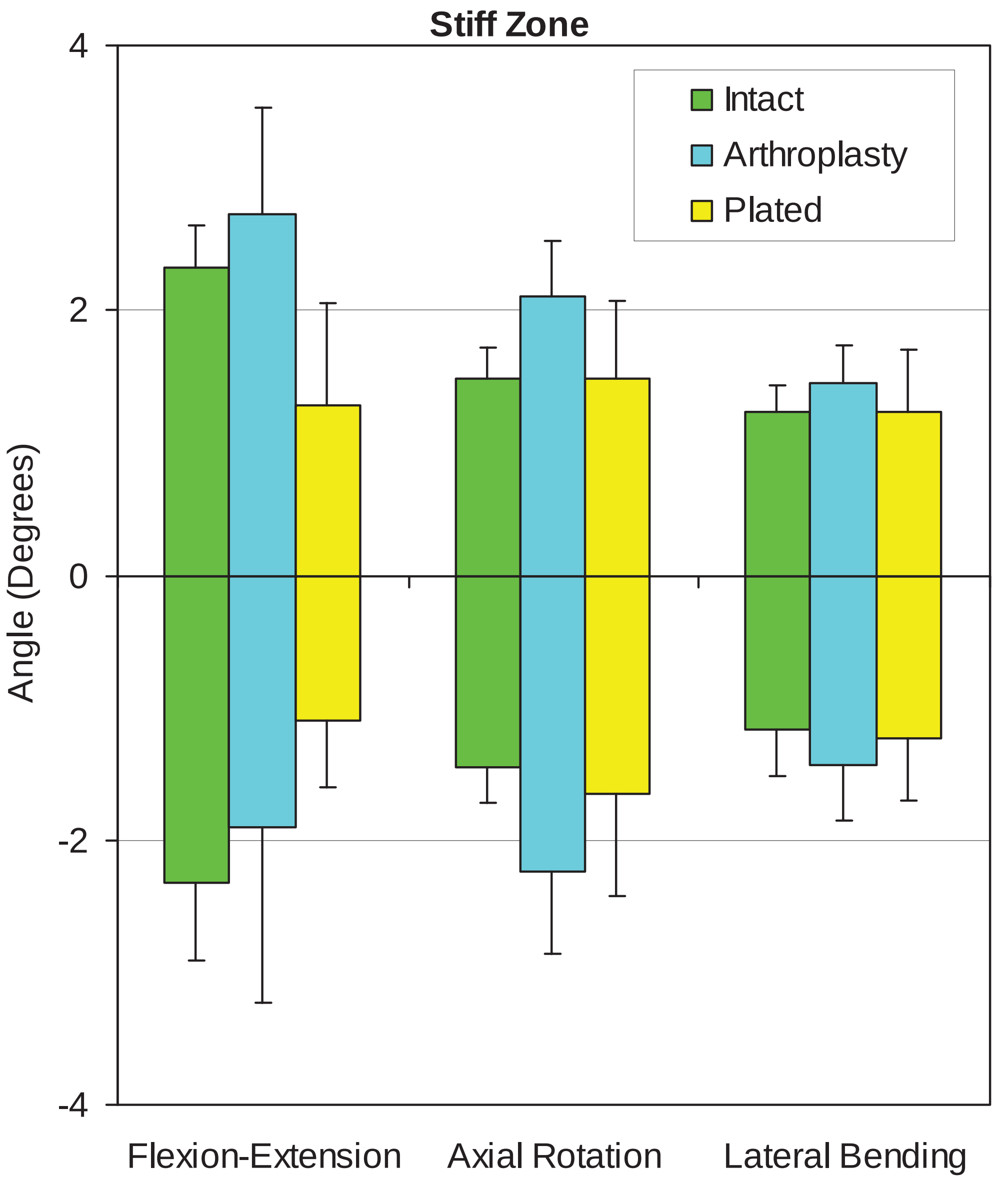

Figure 12. Mean unidirectional angular stiff zone (SZ) at C4-C5 in each condition studied. Error bars show standard deviation.

Table 10. Percent difference in SZ relative to intact (±standard deviation). These differences are % of average.

Loading Mode	Titania	Plated
Flexion	116%±26%	55%±32%
Extension	81%±49%	50%±23%
Axial Rotation	149%±32%	107%±40%
Lateral Bending	123%±27%	107%±51%

Table 11. P-values from RM-ANOVA/Holm-Sidak tests comparing mean SZ among conditions.

Flexion

	Titania	Plated
Intact	0.114	**<0.001**
Titania		**<0.001**

Extension

	Titania	Plated
Intact	0.288	**0.005**
Titania		**0.046**

Lateral Bending

	Titania	Plated
Intact	0.202	0.202
Titania		0.202

Axial Rotation

	Titania	Plated
Intact	**<0.001**	0.523
Titania		**0.002**

Highlighted values represent significant differences ($p<0.05$).

Angular Coupling

The coupling between axial rotation and lateral bending was strong at C5-C6. In intact specimens, 0.59° of coupled axial rotation was observed per degree of lateral bending (Table 12, Figure 13) and 0.56° of coupled lateral bending was observed per degree of axial rotation (Table 13, Figure 13). With Titania disc insertion, both of these coupling patterns were reduced significantly relative to the intact condition ($p<0.03$, Table 14). With plating, both of these coupled motions were even more significantly reduced relative to intact ($p<0.002$, Table 14). With Titania insertion, the coupling was altered less relative to intact than it had been altered with the plate, especially for axial rotation during lateral bending, where the coupling ratio was significantly different between Titania and plate ($p=0.002$, Table 14).

Table 12. Coupled axial rotation during lateral bending at C5-C6 (mean ± standard deviation).

Parameter	Intact	Titania	Plated
Main (LB) Angle (°)	4.95±0.70	2.00±0.70	1.80±0.92
Coupled (AR) Angle (°)	-2.92±1.06	-0.87±0.75	-0.34±0.48
Coupling Ratio	0.59±0.20	0.41±0.28	0.13±0.21

Note: ratio is average of individual ratios, which may differ from ratio of averages.

Table 13. Coupled lateral bending during axial rotation at C5-C6 (mean ± standard deviation).

Parameter	Intact	Titania	Plated
Main (AR) Angle (°)	5.76±0.83	3.45±1.11	2.50±1.36
Coupled (LB) Angle (°)	-3.17±0.73	-1.38±0.48	-0.87±0.64
Coupling Ratio	0.56±0.13	0.42±0.14	0.34±0.12

Note: ratio is average of individual ratios, which may differ from ratio of averages.

Table 14. P-values from RM-ANOVA/Holm-Sidak tests comparing mean coupling ratios.

	Axial Rotation during Lateral Bending			**Lateral Bending during Axial Rotation**	
	Titania	Plated		Titania	Plated
Intact	**0.027**	**0.001**	Intact	**0.029**	**0.002**
	Titania	**0.002**		Titania	0.166

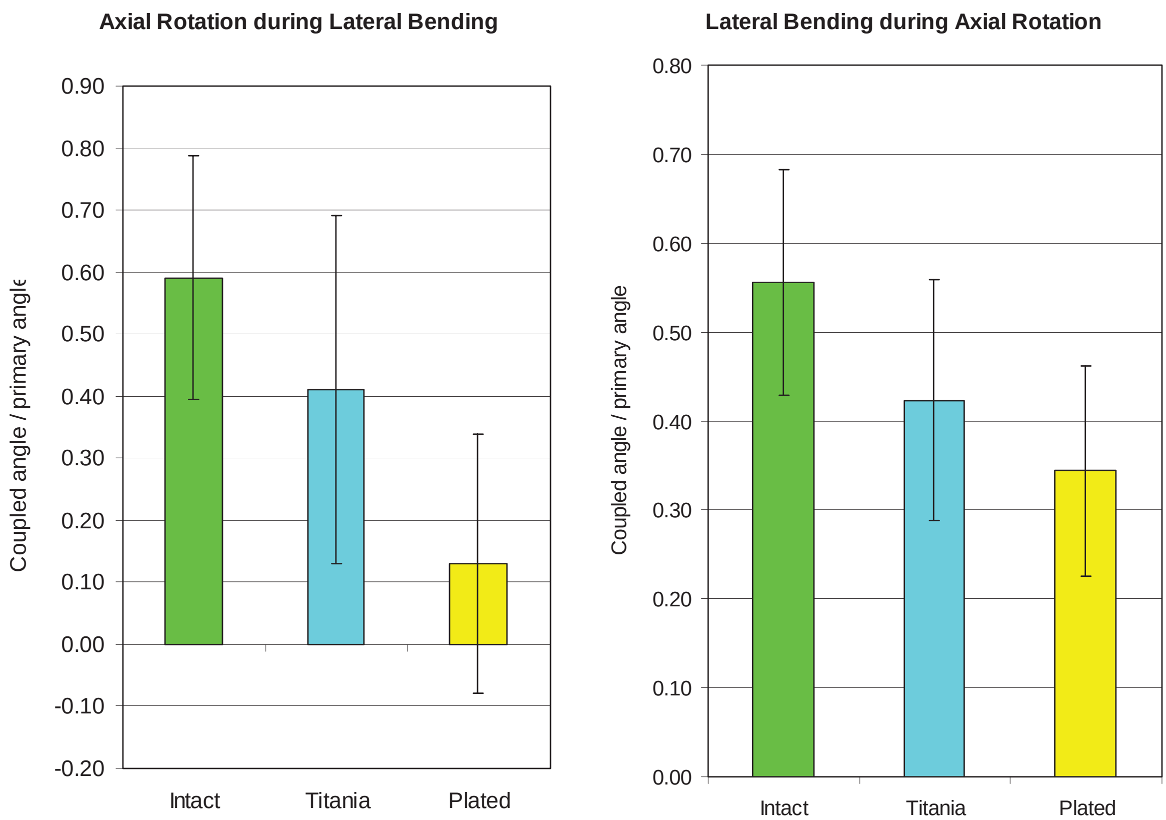

Figure 13. Angular coupled rotation at C5-C6 demonstrating the coupling pattern between lateral bending and axial rotation. Error bars show standard deviation.

Axis of Rotation

After Titania placement, the mean axis of rotation through the midsagittal plane at C5-C6 (index level) during flexion-to-extension shifted anteriorly and rostrally from its intact position (Table 15, Figure 14), however this shift was not significant ($p>0.18$, Table 16). Similarly, after anterior plating the axis of rotation at C5-C6 shifted to a position more rostral and anterior than intact (Table 15, Figure 14); this shift was significant in the rostral direction ($p=0.008$, Table 16). After disc replacement, a significant anterior shift in the position of the axis of rotation was found at the adjacent rostral level ($p=0.001$). No significant shift was seen at the rostral adjacent level after anterior plating ($p>0.16$). There were no significant shifts in the IAR at the adjacent caudal level relative to intact after disc replacement ($p>0.31$), or plating ($p>0.10$).

Table 15. Mean location of the sagittal plane axis of rotation ± standard deviation during flexion-to-extension.

Level	Condition	Anteroposterior Position (mm)	Rostrocaudal Position (mm)
C4-C5	Intact	-11.3±2.1	-7.7±1.5
	Titania	-9.0±2.5	-7.7±1.4
	Plated	-10.5±2.1	-8.3±3.5
C5-C6	Intact	-11.2±2.4	-7.1±2.0
	Titania	-9.4±5.0	-5.1±3.2
	Plated	-10.0±8.4	-2.5±5.6
C6-C7	Intact	-10.7±1.4	-5.5±2.2
	Titania	-9.5±2.5	-5.5±1.9
	Plated	-12.7±2.0	-5.9±1.8

Table 16. P-values from RM-ANOVA/Holm-Sidak tests comparing mean position of axis of rotation among conditions.

C4-C5 – Adjacent Rostral Level

Anteroposterior Position

	Titania	Plated
Intact	**0.001**	0.166
Titania		**0.019**

Rostrocaudal Position

	Titania	Plated
Intact	0.700	0.700
Titania		0.700

C5-C6 – Index Level

Anteroposterior Position

	Titania	Plated
Intact	0.781	0.781
Titania		0.781

Rostrocaudal Position

	Titania	Plated
Intact	0.186	**0.008**
Titania		0.117

C6-C7 – Adjacent Caudal Level

Anteroposterior Position

	Titania	Plated
Intact	0.314	0.104
Titania		**0.015**

Rostrocaudal Position

	Titania	Plated
Intact	0.653	0.653
Titania		0.653

Highlighted values represent significant differences (p<0.05).

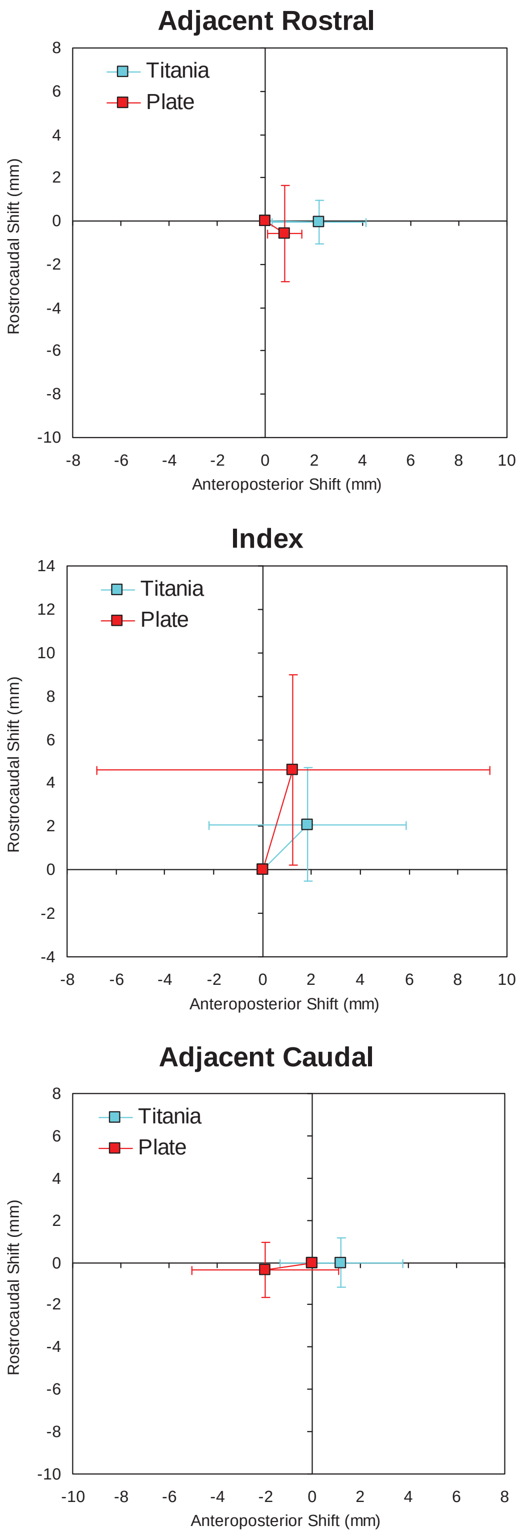

Figure 14. Mean shift in the location of the axis of rotation in the sagittal plane during extension-to-flexion at index (C5-C6), adjacent rostral (C4-C5) and caudal (C6-C7) levels.

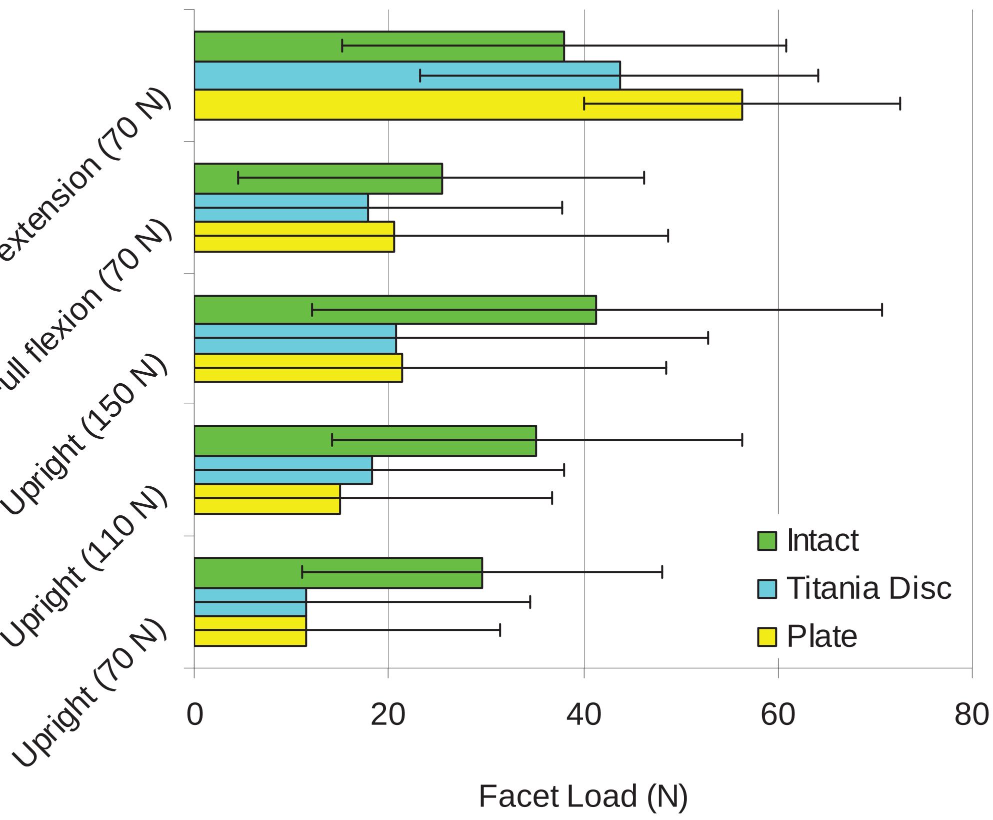

Figure 16. Mean facet loads for different conditions during testing using the belt apparatus with addition of a follower load. Facet loads during flexion and extension are averages of right and left sides. Error bars show standard deviation.

Table 18. P-values from RM-ANOVA/Holm-Sidak tests comparing mean facet loads among conditions.

Flexion

	Titania	Plated
Intact	0.437	0.437
Titania		0.437

Extension

	Titania	Plated
Intact	0.546	0.546
Titania		0.546

Flexion (with follower)

	Titania	Plated
Intact	0.467	0.467
Titania		0.467

Extension (with follower)

	Titania	Plated
Intact	0.340	0.340
Titania		0.340

Lateral Bending (no follower) (contralateral side)

	Titania	Plated
Intact	0.363	0.363
Titania		0.363

Lateral Bending (no follower) (ipsilateral side)

	Titania	Plated
Intact	0.102	0.102
Titania		0.102

Axial Rotation (no follower) (contralateral side)

	Titania	Plated
Intact	0.190	0.190
Titania		0.190

Axial Rotation (no follower) (ipsilateral side)

	Titania	Plated
Intact	0.201	0.201
Titania		0.201

Highlighted values represent significant differences (p<0.05).

Table 19. P-values from RM-ANOVA/Holm-Sidak tests comparing mean facet loads among conditions.

Upright (70 N follower load)

	Titania	Plated
Intact	**0.004**	**0.004**
Titania		0.997

Upright (110 N follower load)

	Titania	Plated
Intact	**0.028**	**0.011**
Titania		0.694

Upright (150 N follower load)

	Titania	Plated
Intact	**0.024**	**0.027**
Titania		0.951

Highlighted values represent significant differences (p<0.05).

During flexion and no follower load, the mean facet load location point shifted slightly laterally, but significantly so, after Titania insertion ($p<0.03$) and plating ($p<0.03$), (Figure 17A, Tables 20 and 21). The addition of a follower load moved the load location point significantly more anteriorly for the plated vs. the disc implanted configuration ($p<0.02$), however neither configuration had a significantly different load location point than intact ($p>0.10$). During extension and no follower load, there was a trend for the load location point to be more posterior after disc insertion than during intact and after plating (Figure 17B). However, this shift was not statistically significant ($p>0.05$, Table 20). The addition of a follower load during extension caused the load location point to shift laterally after both disc insertion ($p<0.001$) and plating ($p<0.004$), (Figure 17B, Table 21). However, there was no significant difference in medio-lateral (or antero-posterior) location of the load location point between the disc implanted and plated configurations ($p>0.2$, Tables 20 and 21). The load location points during axial rotation and lateral bending did not change from intact after either implantation system (Figure 18, Tables 20 and 21).

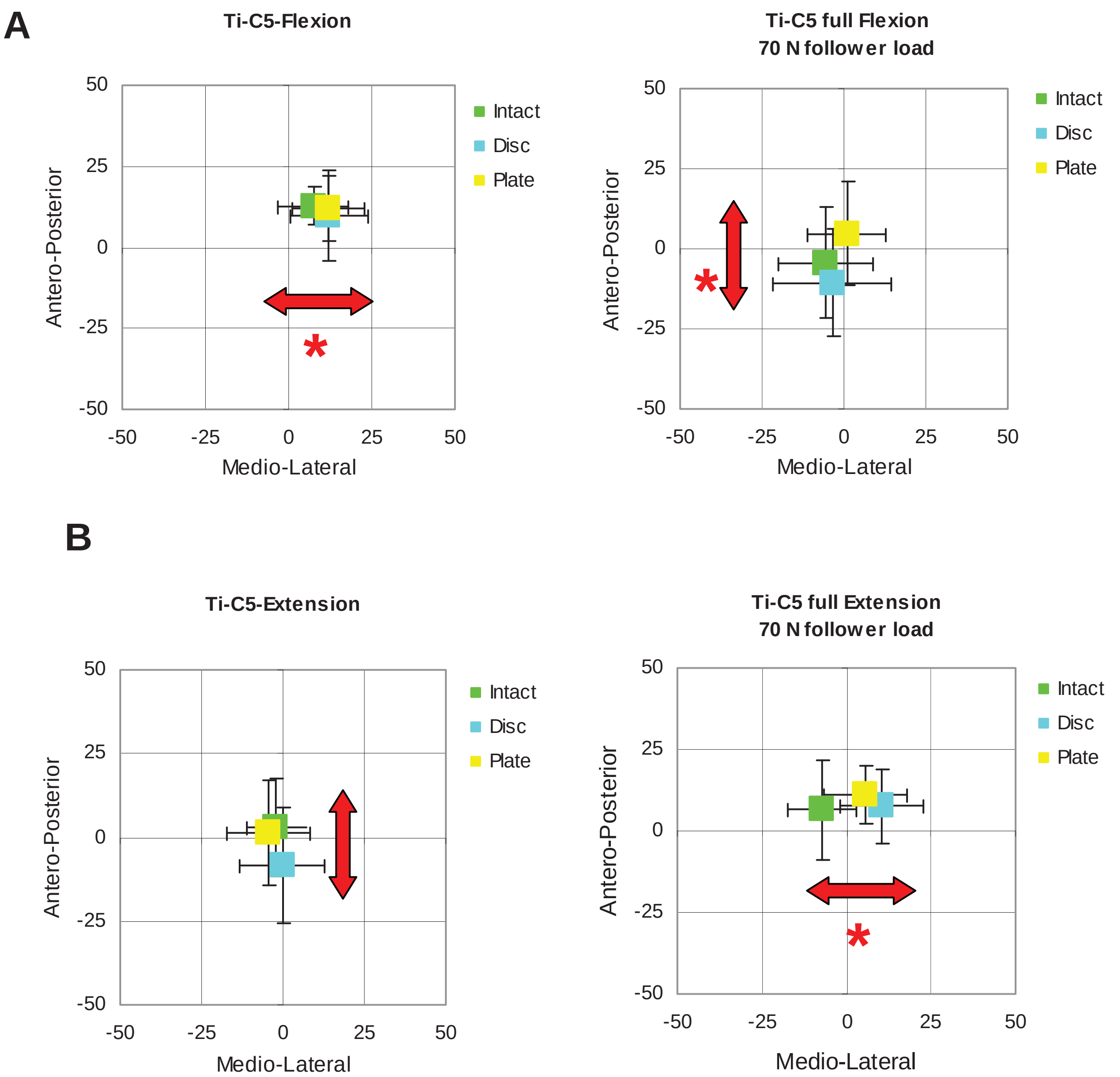

Figure 17. Mean load location points (expressed as percentages of facet dimensions in antero-posterior and mediolateral directions) for different conditions during (A) flexion and (B) extension. The load location points after disc insertion and plating were statistically different from intact in the medio-lateral direction during flexion without a follower load (Titania: p=0.020, plating: p=0.023). Similarly, the load location point after plating was significantly more posterior from that after disc insertion during flexion with a follower load (p=0.010). The load location point shifted posteriorly from intact after disc insertion during extension and without a follower load (p=0.056), and laterally with a follower load (Titania: p<0.001, plating: p=0.003). Error bars show standard deviations. * denotes statistical significance at p<0.05.

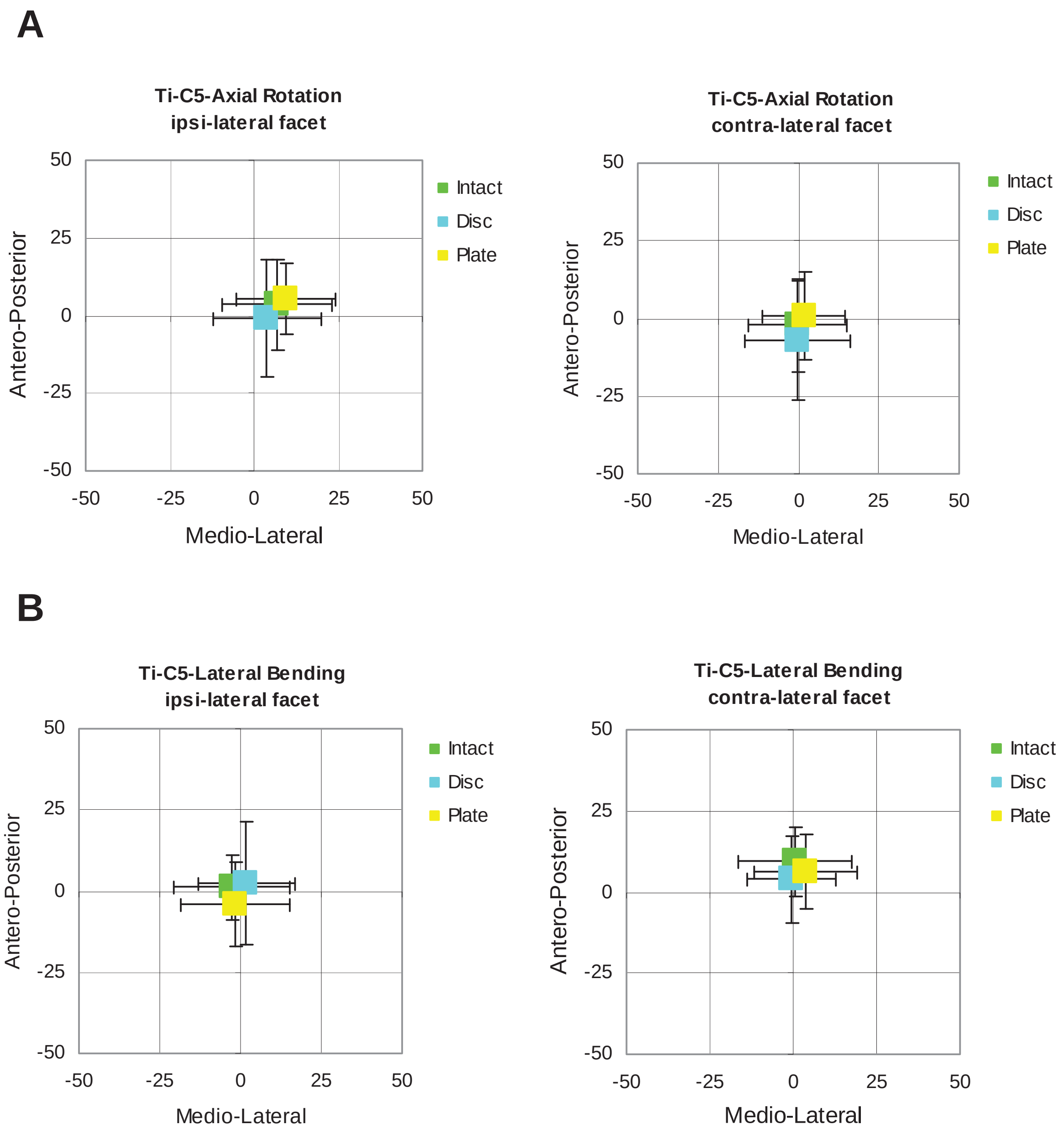

Figure 18. Mean load location points (expressed as percentages of facet dimensions in anteroposterior and mediolateral directions) on contralateral and ipsilateral facets for different conditions during (A) axial rotation and (B) lateral bending. Error bars show standard deviations.

Table 20. P-values from RM-ANOVA/Holm-Sidak tests comparing changes in mean facet load location points in **antero-posterior** direction among conditions.

Flexion

	Titania	Plated
Intact	0.639	0.639
Titania		0.639

Extension

	Titania	Plated
Intact	0.056	0.056
Titania		0.056

Flexion (with follower)

	Titania	Plated
Intact	0.276	0.110
Titania		**0.010**

Extension (with follower)

	Titania	Plated
Intact	0.535	0.535
Titania		0.535

Lateral Bending (no follower) (contralateral side)

	Titania	Plated
Intact	0.376	0.376
Titania		0.376

Lateral Bending (no follower) (ipsilateral side)

	Titania	Plated
Intact	0.347	0.347
Titania		0.347

Axial Rotation (no follower) (contralateral side)

	Titania	Plated
Intact	0.325	0.325
Titania		0.325

Axial Rotation (no follower) (ipsilateral side)

	Titania	Plated
Intact	0.193	0.193
Titania		0.193

Highlighted values represent significant differences (p<0.05).

Table 21. P-values from RM-ANOVA/Holm-Sidak tests comparing changes in mean facet load location points in **medio-lateral** direction among conditions.

Flexion

	Titania	Plated
Intact	**0.020**	**0.023**
Titania		0.939

Extension

	Titania	Plated
Intact	0.386	0.386
Titania		0.386

Flexion (with follower)

	Titania	Plated
Intact	0.354	0.354
Titani Titania	498.25	0.213

Extension (with follower)

	Titania	Plated
Intact	**<0.001**	**0.003**
575.410(Titania	f	0.213 4

0

Segmental Angle Distribution

In determining segmental angle distribution, the global (C3-T1) angle while specimens were loaded in the flexion-compression (stiffness) apparatus was selected that matched the global angle from pure moment (flexibility) testing. After Titania placement, the index level's contribution to global angle decreased significantly during flexion, increased significantly during extension, and decreased significantly during combined flexion-extension (Tables 22-28, Figures 19-22). The plated index level's contribution to global angle also decreased significantly during flexion and flexion-extension (Tables 22-28, Figures 19-22). Differences at the index level between plated and Titania conditions were also significant during extension and flexion-extension but not during flexion (Table 26). After Titania and plate placement, distribution of motion among adjacent levels showed slight but sometimes significant alterations (Figure 23, Tables 29-32).

Table 22. Mean distribution of segmental angles (° ± SD) in the flexion-compression apparatus at global angle matching pure moment tests.

Loading Mode	Level	Intact	Titania	Plated
Flexion	C3-C4	7.0±2.9	7.6±3.3	8.2±2.8
	C4-C5	8.6±1.9	8.9±1.9	8.8±1.8
	C5-C6	8.9±1.7	-4.5±4.2	-4.7±4.4
	C6-C7	7.4±1.8	8.1±1.2	7.6±1.0
	C7-T1	4.0±1.2	4.5±1.2	4.7±1.4
Extension	C3-C4	-6.4±3.1	-6.8±3.5	-7.1±3.6
	C4-C5	-8.3±1.6	-8.8±2.4	-9.9±2.4
	C5-C6	-7.0±1.1	-14.3±1.7	-10.0±3.8
	C6-C7	-4.5±1.3	-5.8±0.9	-6.7±1.9
	C7-T1	1.9±1.2	0.6±1.7	1.1±1.9
Flexion-Extension	C3-C4	13.4±5.7	14.3±6.6	15.2±6.3
	C4-C5	16.9±3.0	17.7±3.0	18.7±3.9
	C5-C6	15.9±2.0	9.8±3.9	5.3±4.4
	C6-C7	12.0±2.5	13.9±1.8	14.3±2.3
	C7-T1	2.1±1.8	3.9±2.6	3.6±2.8

Table 23. Mean distribution of segmental angles (% ± SD) in the flexion-compression apparatus at global angle matching pure moment tests.

Loading Mode	Level	Intact	Titania	Plated
Flexion	C3-C4	19±6	31±14	33±10
	C4-C5	24±5	37±8	37±10
	C5-C6	25±4	-21±20	-22±19
	C6-C7	21±5	34±7	33±8
	C7-T1	11±3	19±7	20±7
Extension	C3-C4	26±9	19±9	22±9
	C4-C5	34±6	25±6	31±4
	C5-C6	29±4	41±6	30±10
	C6-C7	19±6	17±3	21±6
	C7-T1	-8±5	-2±5	-3±5
Flexion-Extension	C3-C4	22±7	24±9	26±8
	C4-C5	28±5	30±4	33±5
	C5-C6	26±3	16±6	8±4
	C6-C7	20±4	24±4	26±5
	C7-T1	3±3	7±5	6±5

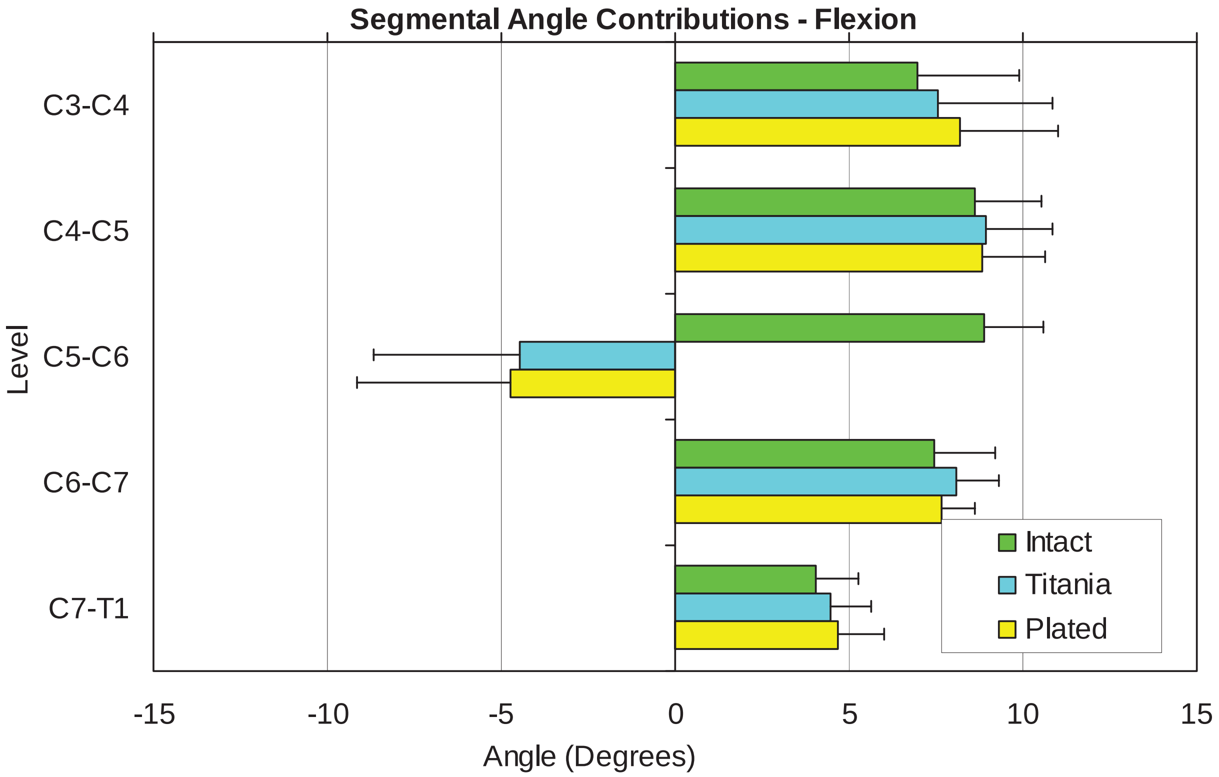

Figure 19. Segmental angle contributions (in degrees) during flexion with follower load at global angle matching pure moment tests. Error bars show standard deviations.

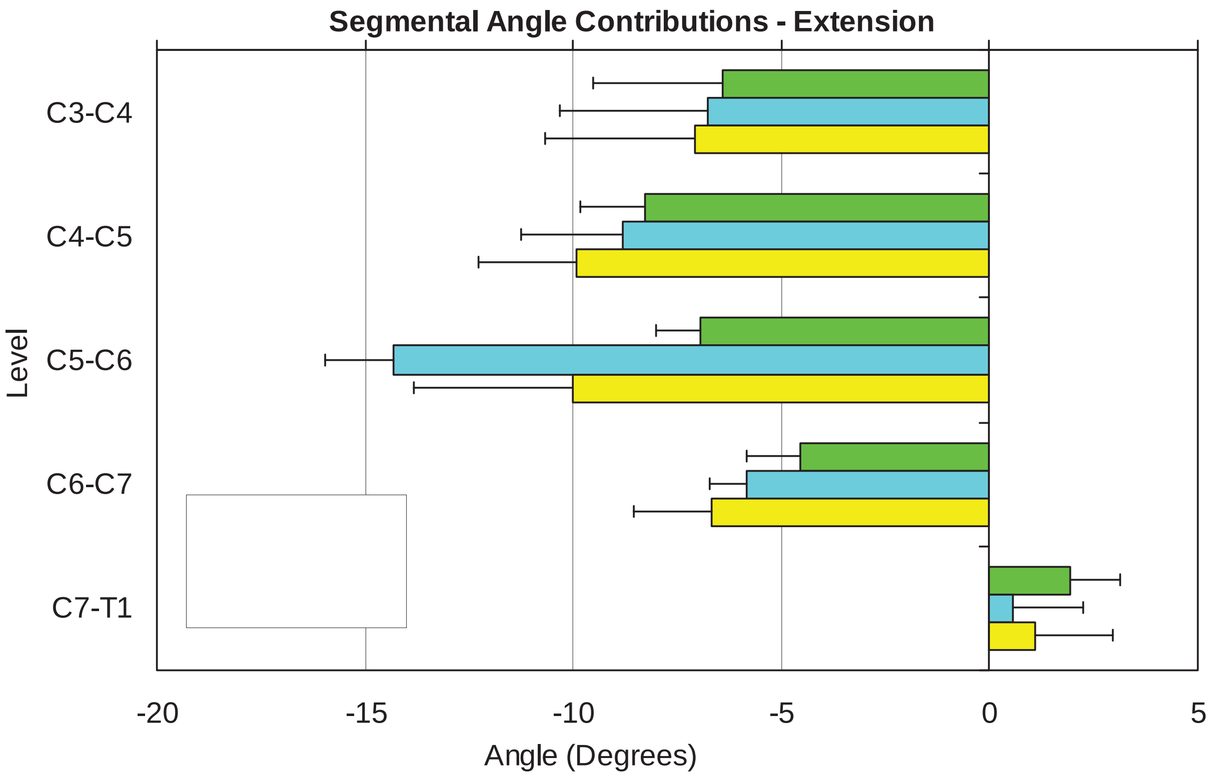
Segmental Angle Contributions - Extension
C3-C4
C4-C5
C5-C6
C6-C7
C7-T1
Level
-20
-15
-10
-5
0
5
Angle (Degrees)

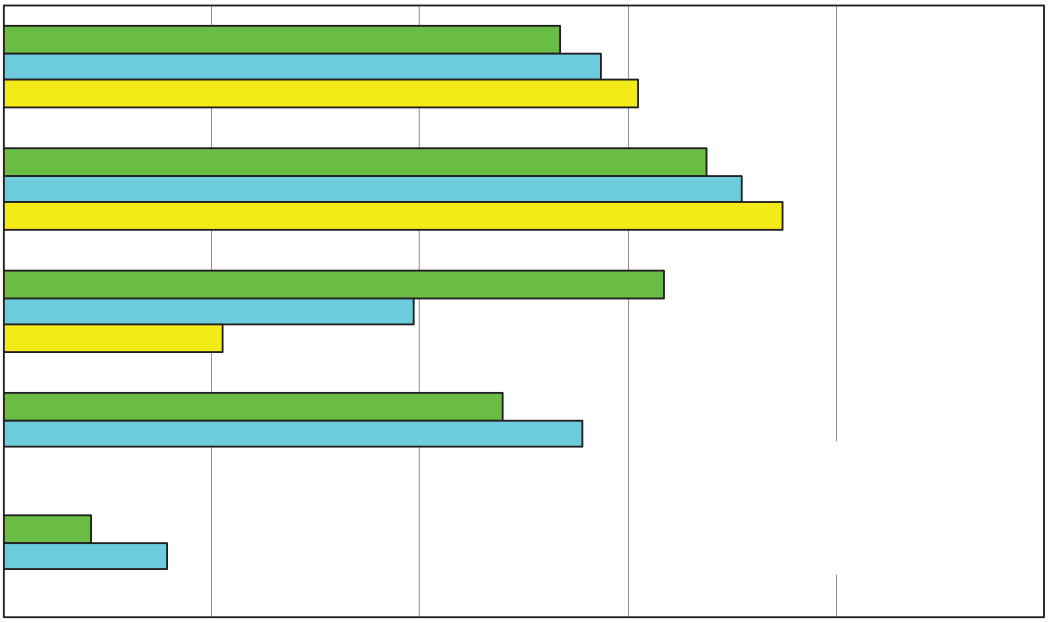

Table 24. P-values from RM-ANOVA/Holm-Sidak tests comparing mean C3-C4 segmental angle among different configurations.

Flexion	Titania	Plated
Intact	0.145	**0.007**
Titania		0.133

Extension	Titania	Plated
Intact	0.202	0.202
Titania		0.202

Flexion-Extension	Titania	Plated
Intact	0.060	**0.001**
Titania		0.068

T i n i a n 3 9 8 9 5 5 (5 (0 . 0 6 8) 3 8 6 0 (

Highlighted values represent significant differences (p<0.05).

\- P **Table 25.** P-values from RM-ANOVA/Holm-Sidak tests comparing mean C4-C5 segmental angle among different configurations. *Flexion* *Extension*

Flexion	Titania	Plated
	26	006 ed
Intact	0.794	0.794

Extension	Titania	Plated			
Intact	0.0	f	4f	218.35	575.44

Intact 0.060

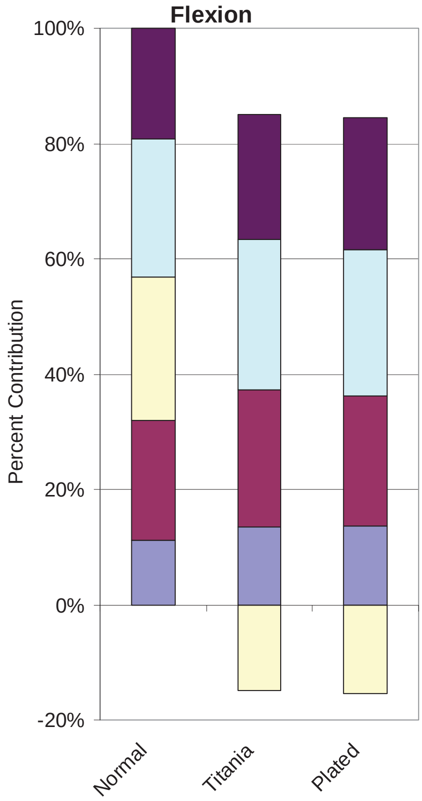

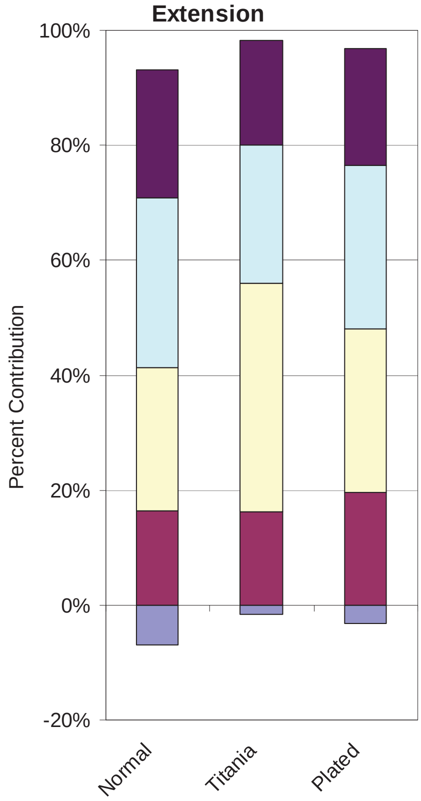

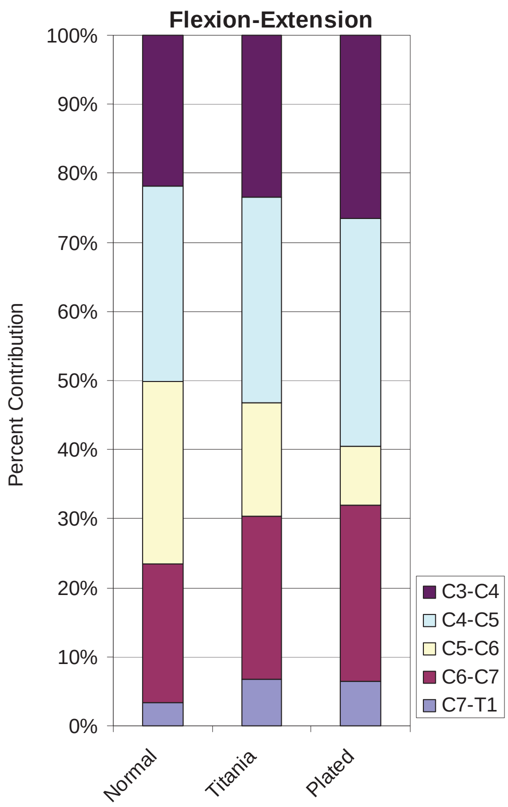

Figure 22. Segmental angle contributions (in %) during flexion, extension, and flexion-extension with follower load at global angle matching pure moment tests.

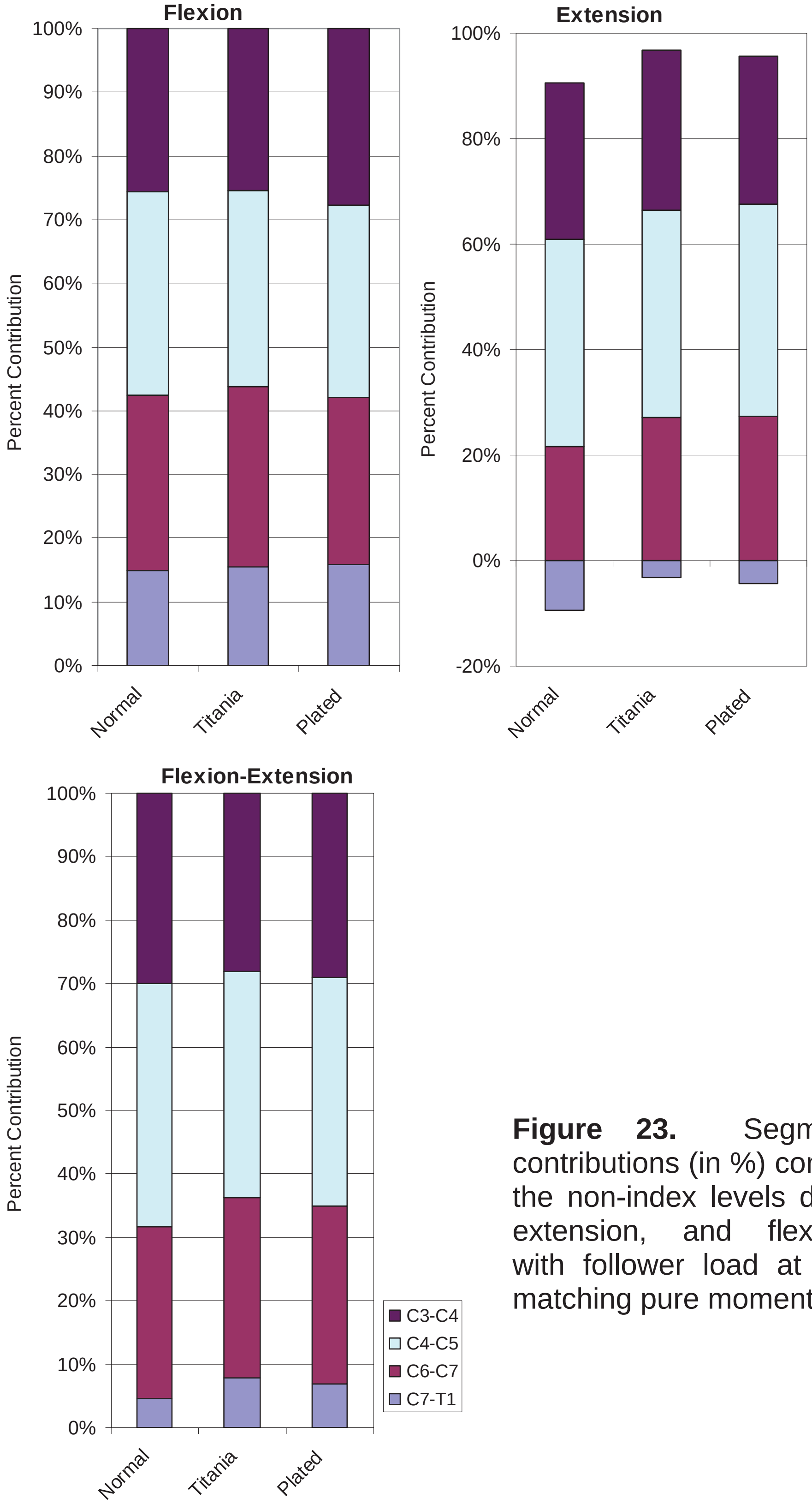

Figure 23. Segmental angle contributions (in %) considering only the non-index levels during flexion, extension, and flexion-extension with follower load at global angle matching pure moment tests.

Table 29. P-values from RM-ANOVA/Holm-Sidak tests comparing mean C3-C4 % contribution (relative to all non-index levels) among different configurations.

Flexion

	Titania	Plated
Intact	0.088	0.088
Titania		0.088

Extension

	Titania	Plated
Intact	0.071	0.071
Titania		0.071

Flexion-Extension

	Titania	Plated
Intact	**0.011**	0.182
Titania		0.148

Highlighted values represent significant differences (p<0.05).

Table 30. P-values from RM-ANOVA/Holm-Sidak tests comparing mean C4-C5 % contribution (relative to all non-index levels) among different configurations.

Flexion

	Titania	Plated
Intact	0.187	0.187
Titania		0.187

Extension

	Titania	Plated
Intact	**0.006**	0.057
Titania		0.250

Flexion-Extension

	Titania	Plated
Intact	**0.010**	**0.022**
Titania		0.714

Highlighted values represent significant differences (p<0.05).

Table 31. P-values from RM-ANOVA/Holm-Sidak tests comparing mean C6-C7 % contribution (relative to all non-index levels) among different configurations.

Flexion

	Titania	Plated
Intact	0.293	0.293
Titania		0.293

Extension

	Titania	Plated
Intact	0.169	0.169
Titania		0.169

Flexion-Extension

	Titania	Plated
Intact	0.301	0.301
Titania		0.301

Table 32. P-values from RM-ANOVA tests comparing mean C7-T1 % contribution (relative to all non-index levels) among different configurations.

Flexion

	Titania	Plated
Intact	0.387	0.387
Titania		0.387

Extension

	Titania	Plated
Intact	**0.005**	**0.017**
Titania		0.559

Flexion-Extension

	Titania	Plated
Intact	**0.003**	**0.019**
Titania		0.349

Highlighted values represent significant differences (p<0.05).

Discussion and Conclusions

Range of Motion, Lax Zone, and Stiff Zone

The sagittal plane (flexion and extension) was the plane that showed the most variability among specimens in the amount of ROM, LZ, and SZ allowed by the disc prosthesis. That is, the standard deviations were greatest in this plane (Figures 10, 11, 12). Thus, the device's performance during sagittal plane motion appears to be most strongly affected by variations in the anatomy and preparation of the disc site. Sagittal plane ROM and LZ were significantly reduced relative to intact by the artificial disc, matching closer the motion allowed by plating. However, sagittal plane SZ with the artificial disc in place was not significantly different than intact. This finding indicates that the mechanical response of the ligaments stretching and the artificial disc articulating, once under substantial loading, is similar to the mechanical response of the natural disc as motion approaches its limits.

There was a significant decrease in transverse plane ROM (axial rotation) after Titania insertion (Figure 10, Table 5). In terms of the subcomponents of mobility (ROM=LZ+SZ, Figure 9), there was a decrease in LZ ($p<0.001$) and an increase in SZ ($p<0.001$) with the artificial disc in place, indicating that the limits to motion were closer to upright than they had been with the intact disc, but that once these limits were engaged, the mechanical response was actually more flexible. The LZ and ROM decreased significantly with the anterior plate in place compared to intact as would be expected with fusion, while the SZ remained unchanged ($p=0.523$, Table 11), indicating only fair purchase at the bone-screw interface. Over time in actual patients, the differences in ROM, LZ, and SZ between artificial disc and fusion would almost certainly become much greater, with ROM, LZ, and SZ all approaching zero for the fused condition.

There was a significant decrease in coronal plane motion (lateral bending) after Titania insertion (Figure 10, Table 5). The LZ decreased ($p<0.001$, Table 8) while the SZ remained unchanged ($p=0.202$, Table 11) after disc insertion, indicating that the earliest resistance to coronal plane motion was met closer to upright than it had been met in the intact condition. However, as motion proceeded, the resistance to further motion matched the response in the intact condition. Response with plating was very similar to the response with the artificial disc, showing no significant differences; lateral bending ROM and LZ with artificial disc versus plate actually matched each other better than ROM and LZ with intact versus artificial disc.

ROM data from the present study can be compared to data involving other artificial discs tested against anterior plating, as presented by others. Chang et al. (2007b) looked at changes in ROM in the cervical spine following insertion of ProDisc-C, Prestige and anterior plating. Motion at C6-C7 (and adjacent levels) was studied during application of 2 Nm pure moment with a simultaneous 100 N compressive pre-load. In contrast to the current study, they found significant increases in ROM at the operated level during flexion, extension, rotation and bending after artificial disc insertion (ProDisc-C and Prestige). It is possible that the different findings are related to differences in prosthesis design or test method such as their use of compressive pre-load. As in the current study and as would be expected intuitively, they also found that plating caused decreased ROM.

Previous (unpublished) results for other devices tested in the same lab as the current tests are more directly comparable. These previous findings also showed different results than were observed for Titania using the same methods. Unlike the current findings for Titania disc, the ROM for ProDisc-C, Prestige, and Bryan was maintained during flexion-extension (Figure 24). Slight reductions in ROM during lateral bending and axial rotation were also observed for ProDisc-C and Prestige, but these reductions were not as severe as for the Titania.

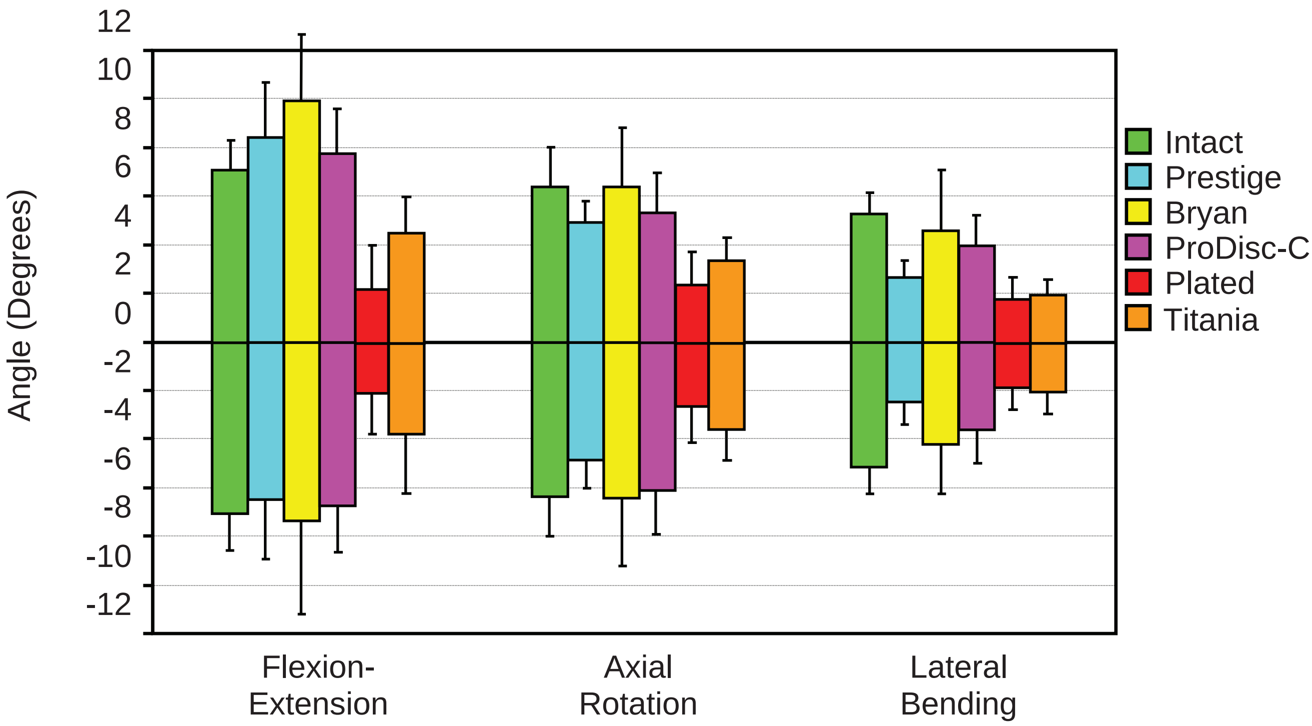

Figure 24. Comparison of range of motion (ROM) for the Titania versus previously tested devices in the same laboratory.

Angular Coupling

It is known that, in the human cervical spine, there is normally a pattern of strong coupling between lateral bending and axial rotation such that coupled lateral bending occurs simultaneously during axial rotation and similarly, coupled axial rotation occurs simultaneously during lateral bending.

It was found in this experiment that the coupling pattern of coupled axial rotation occurring during lateral bending and the coupling pattern of lateral bending occurring during axial rotation were altered such that significantly less coupled motion occurred per unit primary motion than in the intact condition (Figure 13, Table 14). This finding is evidence that the Titania is unable to fully maintain this component of spinal kinematics. It is likely that some articulating surfaces of the device design disallow these coupled secondary motions from occurring. These findings are similar to those observed for other cervical artificial discs (Table 33), which typically have difficulty maintaining consistent normal coupling, especially coupled lateral bending during axial rotation.

Table 33. Index-level coupling factors (coupled motion/primary motion) for cadaveric cervical spines implanted with disc prostheses. P-values are from ANOVA/Holm-Sidak.

Device	Coupled ºLB per ºAR	p-value vs. intact	Coupled ºAR per ºLB	p-value vs. intact
Prestige	0.39±0.08	**0.002**	0.33±0.42	0.093
Bryan	0.50±0.09	0.273	0.38±0.44	0.248
ProDisc-C	0.38±0.18	**0.002**	0.82±0.30	0.149
Titania	0.42±0.14	**0.029**	0.41±0.28	**0.027**

*Values in **boldface** are statistically significant ($p<0.05$).*

Axis of Rotation

It was found that Titania insertion did not affect the position of the flexion-extension axis of rotation at the index level ($p>0.18$, Table 16), but there was a shift at the adjacent rostral level in the anterior direction ($p=0.001$, Figure 14, Tables 15 and 16). This finding probably occurred because specimens instrumented with the Titania were typically placed into a more lordotic orientation, causing the loading vectors to be altered. Anteroposterior position of the axis of rotation is highly dependent upon depth of insertion of the device (not quantified) and device size, and the slight disagreement between Titania-inserted and intact conditions in the anteroposterior position of the IAR indicates that insertion depth was probably very good on average, although a slightly deeper insertion could have prevented even this small shift. It was found that the shift in IAR caused by the Titania was slightly less than the shift in IAR caused by ProDisc-C, Prestige, or Bryan in the same lab.

Facet Loads

For plating, an increase in facet load is relatively unimportant since fusion is the goal. However, no increase in facet load is desirable for the artificial disc. It is also desirable that the mean point of load transmission remain unchanged. In this study, neither Titania insertion nor anterior plating caused significant increases in the magnitude of load distribution via the facets compared to intact during pure moment loading. However, during upright loading with the belt apparatus, both Titania and plating reduced the load to the facets. This finding indicates that the disc height was likely greater after disc insertion than it had been during the intact condition, causing the facets to be distracted and not to experience as much load as they experienced in the intact condition.

Some changes in mean location on the face of the facet of the load were noted without changes in load magnitude (Tables 20 and 21). This finding suggests that changes in kinematic parameters (i.e., ROM, LZ and SZ) caused by implants do not necessarily correlate with changes in the magnitude of load transmission, but possibly with changes in where the loads are being transmitted. However, more data are necessary before further conclusions can be drawn in this regard.

Segmental Angle Distribution

During unilateral flexion or unilateral extension with the belt apparatus, the contribution of the Titania-implanted level was markedly different than the intact contribution. This finding occurred because implantation of the Titania caused C5-C6 to go into an extended resting posture. Thus, during extension, C5-C6 was already somewhat extended and, with loading, extended even farther. During flexion, C5-C6 started already extended while upright and therefore had to move back to neutral before going into flexion. While the whole specimen was fully flexed, the C5-C6 level had not (in most specimens) passed through what used to be its $0°$ posture in the intact condition (Figure 19). This finding is evidence that Titania devices may have been too large despite careful sizing by the surgeons.

It was found that the Titania-implanted spines had bilateral (flexion-extension) segmental angle distributions that were closer to intact at the index and adjacent levels than with plating. That is, for a given global angle (measured C3-T1), the breakdown of segmental angles at C3-C4, C4-C5, C5-C6, C6-C7 and C7-T1 was altered less from the normal, intact breakdown of segmental angles (flexion-extension plot, Figure 22). A large contribution to flexion-extension was still seen at the index level after plating. However, as mentioned earlier, plating was not effective in completely immobilizing specimens. The difference in segmental angle contribution would certainly be greater clinically after fusion.

Summary

The Titania and anterior plating both altered cervical biomechanics although in different ways (Table 34). In general, deviations from intact were less substantial after artificial disc placement than after plating. This information extends the understanding of how the Titania disc implant behaves and aids in comparing the Titania to other artificial discs.

Table 34. Summary of alterations relative to intact condition observed for Titania-implanted and plated conditions.

Parameter	Titania-implanted	Plated
Range of motion - Flexion	**- -**	**- -**
Range of motion - Extension	**- -**	**- -**
Range of motion - Lateral Bending	**- -**	**- -**
Range of motion - Axial Rotation	**- -**	**- -**
Lax zone - Flexion-Extension	**- -**	**- -**
Lax zone - Lateral Bending	**- -**	**- -**
Lax zone - Axial Rotation	**- -**	**- -**
Stiff zone - Flexion		**- -**
Stiff zone - Extension		**- -**
Stiff zone - Lateral Bending		
Stiff zone - Axial Rotation	**+**	
Coupled Ax. Rot. during Lat. Bend.	**-**	**- -**
Coupled Lat. Bend. during Ax. Rot.	**-**	**- -**
Anteroposterior position of axis of rotation		
Rostrocaudal position of axis of rotation		**+**
Facet load during flexion-extension		
Facet load during other loading	**-**	**-**
Facet load location point during flexion-extension	**+**	**+**
Facet load location point during other loading		
Segmental angle distribution (%)	**-**	**- -**

Blank = no change, **+** = mild increase, **+ +** = substantial increase, **-** = mild decrease, **- -** = substantial decrease.

References

1. Chang UK, Kim DH, Lee MC, Willenberg R, Kim SH, Lim J: Changes in adjacent-level disc pressure and facet joint force after cervical arthroplasty compared with cervical discectomy and fusion. **J Neurosurg Spine 7(1)**:33-39, 2007a.
2. Chang UK, Kim DH, Lee MC, Willenberg R, Kim SH, Lim J: Range of motion change after cervical arthroplasty with ProDisc-C and Prestige artificial discs compared with anterior cervical discectomy and fusion. **J Neurosurg Spine 7(1)**:40-46, 2007b.
3. Crawford NR, Brantley AGU, Dickman CA, Koeneman EJ: An apparatus for applying pure nonconstraining moments to spine segments *in vitro*. **Spine 20(19)**:2097-2100, 1995.
4. Crawford NR, Dickman CA: Construction of local vertebral coordinate systems using a digitizing probe. Technical note. **Spine 22(5)**:559-563, 1997.
5. Crawford NR, Peles JD, Dickman CA: The spinal lax zone and neutral zone: measurement techniques and parameter comparisons. **J Spinal Disord 11(5)**:416-429, 1998.
6. Crawford NR, Yamaguchi GT, Dickman CA: A new technique for determining 3-D joint angles: the tilt/twist method. **Clin Biomech (Bristol, Avon) 14(3)**:153-165, 1999.
7. Crawford NR: Analysis: In vitro biomechanical construct tests evaluating cervical arthroplasty. **World Spine Journal 1(1)**:7-13, 2006.
8. DiAngelo DJ, Foley KT, Vossel KA, Rampersaud YR, Jansen TH: Anterior cervical plating reverses load transfer through multilevel strut-grafts. **Spine 25(7)**:783-795, 2000.
9. DiAngelo DJ, Roberston JT, Metcalf NH, McVay BJ, Davis RC: Biomechanical testing of an artificial cervical joint and an anterior cervical plate. **J Spinal Disord Tech 16(4)**:314-323, 2003.
10. DiAngelo DJ, Foley KT, Morrow BR, Schwab JS, Song J, German JW, Blair E: In vitro biomechanics of cervical disc arthroplasty with the ProDisc-C total disc implant. **Neurosurg Focus 17(3)**:E7, 2004.
11. Dmitriev AE, Cunningham BW, Hu N, Sell G, Vigna F, McAfee PC: Adjacent level intradiscal pressure and segmental kinematics following a cervical total disc arthroplasty: an in vitro human cadaveric model. **Spine 30(10)**:1165-1172, 2005.
12. Hu N, Cunningham BW, McAfee PC, Kim SW, Sefter JC, Cappuccino A, Pimenta L: Porous coated motion cervical disc replacement: a biomechanical, histomorphometric, and biologic wear analysis in a caprine model. **Spine 31(15)**:1666-1673, 2006.
13. Kotani Y, Cunningham BW, Abumi K, Dmitriev AE, Ito M, Hu N, Shikinami Y, McAfee PC, Minami A: Multidirectional flexibility analysis of cervical artificial disc

reconstruction: in vitro human cadaveric spine model. **J Neurosurg Spine 2(2)**:188-194, 2005.

14. McAfee PC, Cunningham B, Dmitriev A, Hu N, Woo Kim S, Cappuccino A, Pimenta L: Cervical disc replacement-porous coated motion prosthesis: a comparative biomechanical analysis showing the key role of the posterior longitudinal ligament. **Spine 28(20S)**:S176-185, 2003.
15. Panjabi MM: Biomechanical evaluation of spinal fixation devices: I. A conceptual framework. **Spine 13(10)**:1129-1134, 1988.
16. Puttlitz CM, Rousseau MA, Xu Z, Hu S, Tay BK, Lotz JC: Intervertebral disc replacement maintains cervical spine kinetics. **Spine 29(24)**:2809-2814, 2004.
17. Sawa AGU, Crawford NR: The use of surface strain data and a neural networks solution method to predict lumbar facet joint loads during in vitro spine testing. **J Biomech 41(12)**:2647-2653, 2008.
18. Spoor CW, Veldpaus FE: Rigid body motion calculated from spatial co-ordinates of markers. **J Biomech 13(4)**:391-393, 1980.

Not:

Not: